2010 IEEE International Conference on Robotics and Automation
Anchorage Convention District
May 3-8, 2010, Anchorage, Alaska, USA

Control Strategies for Ankle Rehabilitation using a High Performance Ankle Exerciser

Saglia, J. A., Tsagarakis, N. G., Dai, J. S., and Caldwell, D. G.

Abstract—**This paper presents the control architecture and preliminary experimental results of a high performance parallel robot used for ankle rehabilitation. The goal of this work was to design suitable control algorithms for diagnostic, training and rehabilitation of the ankle in presence of musculoskeletal injuries. A position control scheme is used for patient-passive exercises while an admittance control technique is used to perform patient-active exercises with and without motion assistance. The design of the control algorithms is based on the analysis of the rehabilitation protocol taking into account the dynamics of the system and the dynamics of the interaction between the human and the robot. Electromyographic (EMG) signals are used to evaluate patient's effort during training/exercising. The results indicate the great potential of the rehabilitation device as a tool to fasten and improve the ankle therapies outcome.**

I. Introduction

In the last decades several research studies demonstrated that rehabilitation robots have a great potential in improving diagnostics and physiotherapy outcome [1-4]. The main advantages of the automated rehabilitation systems are that they can be used to perform a huge number of repetitions, which was proved to be extremely beneficial in the treatment of neuromuscular injuries [5]. Further, such systems turn out to be extremely precise diagnostic tools and can provide quantitative measures of the patient's recovery state after an injury [6].

Even though there is a strong evidence of the benefits that the rehabilitation robots can provide, their spread is still very limited. However, the development of such systems is attracting interest of the research community and as a result many robots are being built and tested [7].

In parallel with the device developments many control strategies for human-robot interaction, and particularly for rehabilitation purposes, have been proposed and can be found in the literature [8-12], most of which are based on impedance control [13].

Focusing on ankle rehabilitation systems, Girone et al. introduced in 1999 a 6-dof Stewart-Gough platform named the 'Rutgers Ankle'. This system has been described in [14-16] and the first results with stroke patients have been reported in [17]. These studies demonstrated that a platform type rehabilitation device has the potential to improve the physiotherapy outcome. The 'Rutgers Ankle' can be controlled either in position/orientation or force/torque. Later, in 2005 Yoon et al. [18] presented a 4-dof, reconfigurable ankle rehabilitation robot based on a hybrid parallel-serial mechanism. This system was designed to perform strengthening and balance exercises allowing two rotations and one translation for the ankle and, one extra degree of freedom for toes flexion/extension. The study reported also on the control architecture which made use of a position-based impedance control to simulate the desired reference impedance. Preliminary results on the controller performance for different rehabilitation exercises were reported. Other ankle rehabilitation devices were introduced in [19, 20], however no clinical trials have been carried out.

Although all the works mentioned above are well justified and show promising results, none of the existing systems effectively monitors the patient's muscular activity nor integrates such information in its control architecture. While EMG-based controllers are common for wearable rehabilitation robots (e.g. exoskeleton), to the author's knowledge they have never been applied to the control of ankle rehabilitation robots.

The work presented in this paper is implemented on a rehabilitation robot introduced in [21, 22], see Fig. 1.

The aim of this paper is to present the development of the control architecture for this ankle rehabilitation system. The control of the system needs to facilitate all types of exercises foreseen by the rehabilitation protocol [22] and serve as a tool for the physiotherapist to treat patients in a faster and more effective manner. The patient's muscular activity is integrated into the control algorithm through the monitoring of the EMG signals, in order both to achieve effective assistive control and to assist in the evaluation of the exercise outcome.

In this paper, Section II briefly describes the high performance ankle rehabilitation robot while Section III reports on the analysis of dynamics of the interaction. Consequently, Section IV presents the control algorithms and shows how those algorithms are suitable to the needs of the various rehabilitation exercises. Finally, the experimental results are reported in Section V and discussed in Section VI.

II. Ankle Rehabilitation Robot

A. Mechanism Description

Figure 1 demonstrates the ankle rehabilitation robot used

This work was supported by the Istituto Italiano di Tecnologia in collaboration with King's College London.

J. A. Saglia and J. S. Dai are with the Istituto Italiano di Tecnologia, 16163, Genova, Italy and with King's College London, WC2R 2LS, UK, (corresponding author, e-mail: jody.saglia@iit.it).

N. G. Tsagarakis and D. G. Caldwell are with the Istituto Italiano di Tecnologia, 16163, Genova, Italy.

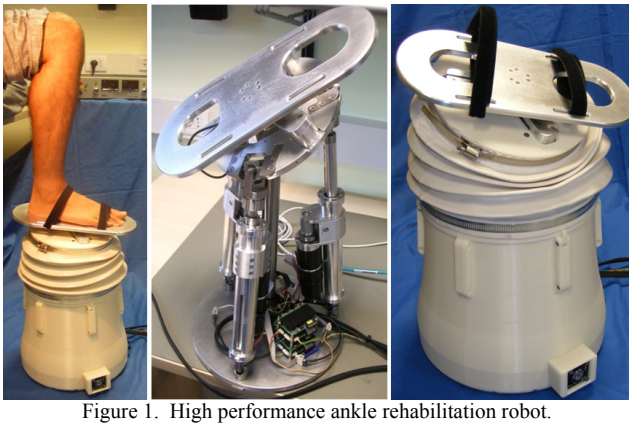

Figure 1. High performance ankle rehabilitation robot.

in this study. The robot is basically a 3UPS/U[1] parallel mechanism with two rotational degrees of freedom. The mechanical structure is composed of a fixed base, a central strut, a moving platform and three actuated limbs with a UPS kinematic chain. The platform is attached to the central strut through a universal joint. As depicted in Fig. 1, the patient's foot is constrained to the footplate with Velcro stripes.

The limb prismatic joint is actuated by a custom designed linear actuator. This actuator makes use of a brushed DC motor Maxon RE40 and a planetary gearbox with a reduction ratio ρ of 12:1. A capstan system of pulleys together with a steel cable transmission transforms the rotary motion of the motor into the linear displacement of the piston. Optical encoders of 4096 ppr mounted on the DC motor shafts provide a position resolution of 1.278 μm at the prismatic joint.

The custom actuator can provide a peak force of over 1100N and a maximum speed of 60cm/s. The resultant maximum device output torque is 120Nm and the maximum speed is 500°/sec. More details on the system can be found in [22].

An ATI 6-axis force/torque (FT) sensor mounted between the moving platform and the footplate senses the human-robot interaction forces and torques. The device is interfaced to a standard PC through a CAN interface. Further, EMG signals relative to plantar/dorsiflexion motion are collected at a frequency of 128 Hz via a Bluetooth link.

III. Dynamics of Interaction

A. Mechanism Kinematics

From [23], the linear velocity of the *i*-th spherical joint, can be expressed in terms of the platform angular velocity as,

$$\boldsymbol{v}_{\mathrm{B}i} = \boldsymbol{\omega}_{\mathrm{P}} \times \boldsymbol{b}_i \,, \tag{1}$$

with i = 1, 2 and 3, where $\boldsymbol{\omega}_{\mathrm{P}}$ is the platform angular velocity and $\boldsymbol{b}_i$ is the position vector of the *i*-th spherical joint, from the platform fixed reference frame to the joint.

Equation (1) can also be expressed in terms of limb linear and angular velocities as,

$$\boldsymbol{v}_{\mathrm{B}i} = \dot{d}_i \boldsymbol{s}_i + d_i \boldsymbol{\omega}_i \times \boldsymbol{s}_i \,, \tag{2}$$

where d_i, $\dot{d}_i$ are the limb (actuator) length and linear velocity respectively, $\boldsymbol{\omega}_i$ is the limb angular velocity and $\boldsymbol{s}_i$ is the unit vector along the limb vertical axis.

Inserting (1) into (2) and rearranging in matrix form yields,

$$\begin{bmatrix} \dot{d}_i \\ \dot{\alpha}_i \\ \dot{\beta}_i \end{bmatrix} = \mathbf{J}_i \begin{bmatrix} \dot{\theta}_{\mathrm{PD}} \\ \dot{\theta}_{\mathrm{EI}} \end{bmatrix}, \tag{3}$$

where $\dot{\alpha}_i$ and $\dot{\beta}_i$ are the time derivatives of the angles of the *i*-th passive universal joint that connects the actuator to the base while $\dot{\theta}_{\mathrm{PD}}$ and $\dot{\theta}_{\mathrm{EI}}$ are the angular velocities of the moving platform relative to plantar/dorsiflexion and eversion/inversion respectively. The limb Jacobian matrix is expressed by $\mathbf{J}_i$, whose dimension is 3 by 2. Combining the first rows of the three limb Jacobian matrices gives the relation between the independent platform angular velocities $\dot{\boldsymbol{q}}_{\mathrm{in}} = [\dot{\theta}_{\mathrm{PD}} \quad \dot{\theta}_{\mathrm{EI}}]^{\mathrm{T}}$ and the actuators linear velocities $\dot{\boldsymbol{q}}_{\mathrm{a}} = [\dot{d}_1 \quad \dot{d}_2 \quad \dot{d}_3]^{\mathrm{T}}$, as,

$$\mathbf{J}_{\mathrm{r}} \dot{\boldsymbol{q}}_{\mathrm{in}} = \dot{\boldsymbol{q}}_{\mathrm{a}} \,, \tag{4}$$

where $\mathbf{J}_{\mathrm{r}}$ is the non-square, 3 by 2 Jacobian matrix of the redundantly actuated parallel mechanism.

The velocity relation between the independent platform angular velocities and the angular velocities of the passive limb universal joints $\dot{\boldsymbol{q}}_{\mathrm{p}} = [\dot{\alpha}_1 \quad \dot{\beta}_1 \quad \dot{\alpha}_2 \quad \dot{\beta}_2 \quad \dot{\alpha}_3 \quad \dot{\beta}_3]^{\mathrm{T}}$ is composed of the second and third rows of the three limb Jacobian matrices $\mathbf{J}_i$, as,

$$\mathbf{J}_{\mathrm{p}} \dot{\boldsymbol{q}}_{\mathrm{in}} = \dot{\boldsymbol{q}}_{\mathrm{p}} \,, \tag{5}$$

where $\mathbf{J}_{\mathrm{p}}$ is a non-square, 6 by 2 Jacobian matrix.

Combining all, active and passive joint variables in a single vector, gives a vector of generalized coordinates as $\boldsymbol{q} = [\boldsymbol{q}_{\mathrm{a}} \quad \boldsymbol{q}_{\mathrm{p}} \quad \boldsymbol{q}_{\mathrm{in}}]^{\mathrm{T}}$ and its time derivative can be related to the independent coordinates as,

$$\dot{\boldsymbol{q}} = \begin{bmatrix} \mathbf{J}_{\mathrm{r}} \\ \mathbf{J}_{\mathrm{p}} \\ \mathbf{I} \end{bmatrix} \dot{\boldsymbol{q}}_{\mathrm{in}} = \mathbf{J} \dot{\boldsymbol{q}}_{\mathrm{in}} \,, \tag{6}$$

where $\mathbf{J}$ is a non-square, 11 by 2 Jacobian matrix.

The acceleration can be obtained differentiating (6) with respect to time, thus obtaining,

$$\ddot{\boldsymbol{q}} = \dot{\mathbf{J}} \dot{\boldsymbol{q}}_{\mathrm{in}} + \mathbf{J} \ddot{\boldsymbol{q}}_{\mathrm{in}} \,. \tag{7}$$

[1] U, P and S stand for universal, prismatic and spherical joint respectively. An underlined letter represents an actuated joint.

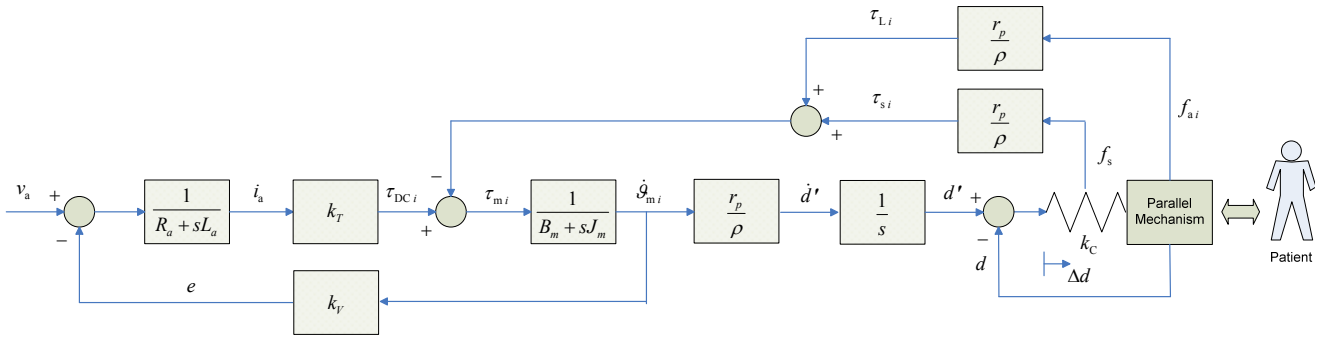

Figure 2. Dynamic model of the custom designed linear actuator in the robotic system interacting with the patient.

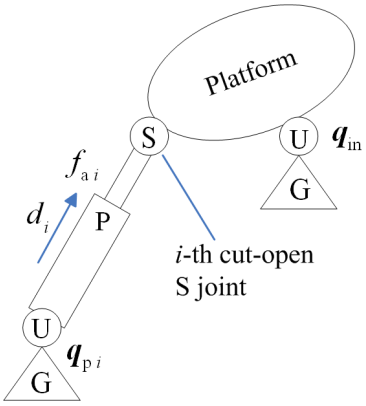

Figure 3. Equivalent kinematic tree. Note, S, U, P and G stand for spherical, universal, prismatic joints and ground.

B. *Mechanism Dynamics*

The dynamics of the redundantly actuated parallel mechanisms can be analyzed by considering the dynamics of an equivalent tree system [24], generated by cut-opening some of the passive joints in order to brake all the kinematic loops, see Fig. 3. In this case, the kinematic loops have been cut at the spherical joints in order to create three identical limb tree systems and a strut/platform tree system. The dynamics of the equivalent tree system is expressed by

$$\mathbf{M}_{\mathrm{t}}(\boldsymbol{q})\ddot{\boldsymbol{q}} + \mathbf{C}_{\mathrm{t}}(\dot{\boldsymbol{q}}, \boldsymbol{q})\dot{\boldsymbol{q}} + \mathbf{N}_{\mathrm{t}}(\boldsymbol{q}) = \boldsymbol{\tau}\,, \tag{8}$$

where $\mathbf{M}_{\mathrm{t}}$, $\mathbf{C}_{\mathrm{t}}$ and $\mathbf{N}_{\mathrm{t}}$ are the Inertia, Coriolis and Centrifugal and eventually Gravity matrices of the tree system respectively. The vector $\boldsymbol{\tau}$ contains forces and torques of the tree system. Note that friction effects have been neglected.

The mapping between the independent platform torques and those of the tree system can be expressed as,

$$\boldsymbol{\tau}_{\mathrm{in}} = \mathbf{J}^{\mathrm{T}}\,\boldsymbol{\tau}\,, \tag{9}$$

while the actuators forces can be mapped to the independent platform torques with the relation,

$$\boldsymbol{\tau}_{\mathrm{in}} = \mathbf{J}_{\mathrm{r}}^{\mathrm{T}}\boldsymbol{f}_{\mathrm{a}}\,. \tag{10}$$

Plugging (6) and (7) into (8) and, consequently in (9) and (10) yields,

$$\mathbf{M}\ddot{\boldsymbol{q}}_{\mathrm{in}} + \mathbf{C}\dot{\boldsymbol{q}}_{\mathrm{in}} + \mathbf{N} = \mathbf{J}_{\mathrm{r}}^{\mathrm{T}}\,\boldsymbol{f}_{\mathrm{a}}\,, \tag{11}$$

where

$$\mathbf{M} = \mathbf{J}^{\mathrm{T}}\mathbf{M}_{\mathrm{t}}\,\mathbf{J}\,,$$
$$\mathbf{C} = \mathbf{J}^{\mathrm{T}}\mathbf{M}_{\mathrm{t}}\,\dot{\mathbf{J}} + \mathbf{J}^{\mathrm{T}}\mathbf{C}_{\mathrm{t}}\,\mathbf{J}\,,$$
$$\mathbf{N} = \mathbf{J}^{\mathrm{T}}\mathbf{N}_{\mathrm{t}}\,.$$

Therefore, the inverse dynamics is given by

$$\boldsymbol{f}_{\mathrm{a}} = \mathbf{J}_{\mathrm{r}}^{+\mathrm{T}}(\,\mathbf{M}\ddot{\boldsymbol{q}}_{\mathrm{in}} + \mathbf{C}\dot{\boldsymbol{q}}_{\mathrm{in}} + \mathbf{N}\,), \tag{12}$$

with $\mathbf{J}_{\mathrm{r}}^{+\mathrm{T}}$ being the pseudo-inverse Jacobian matrix of the redundantly actuated parallel mechanism, computed in the form that minimizes the actuator forces [25-27].

C. *Actuator Dynamics*

The dynamics of the custom linear actuator is composed of the DC motor dynamics, cable transmission and the dynamics of the prismatic joint. However, the mass of the prismatic link has already been included in the equation-of-motion (EoM) of the parallel mechanisms (11).

Therefore, the torque required by the i-th motor can be expressed as

$$\tau_{\mathrm{DC}i} = \tau_{\mathrm{s}\,i} + \tau_{\mathrm{m}\,i} + \tau_{\mathrm{L}\,i}\,, \tag{13}$$

and it is sum of the torque due to non-infinite stiffness of the transmission cable $\tau_{\mathrm{s}\,i}$, the torque due to motor shaft inertia and motor friction $\tau_{\mathrm{m}\,i}$ and the load torque $\tau_{\mathrm{L}\,i}$ which includes the effect of the mechanism dynamics and the load applied by the patient.

The block diagram representing the dynamics of the actuator can be seen in Fig. 2, where B_m, J_m, R_a, L_a, k_T and k_V are the mechanical, electric and constant characteristics of the electric DC motor. The radius of the motor pulley r_p relates the torque produced by the DC motor with output force produced at the actuator tip.

The diagram shows that the electric motor needs to produce a torque $\tau_{\mathrm{DC}i}$ able to counteract, the force generated by the cable transmission such as,

$$\tau_{\mathrm{s}\,i} = k_{\mathrm{C}}\Delta d\,, \tag{14}$$

where k_C is the stiffness of the transmission cable and $\Delta d = d' - d$ with, d' being the linear displacement generated by the rotation of the motor and d the real linear displacement of the prismatic joint, and the forces/torques due to the dynamics of the mechanism and the interaction with the patient $\boldsymbol{f}_{a\,i}$ (the i force component of $\boldsymbol{f}_a$ in (12)).

D. Dynamics of Human-Robot Interaction

The complete dynamics of the robotic system is described by the combination of (12) and (13). In a scenario where the robot is applied to rehabilitation, the interaction between the robot and the human must be included in the dynamic model. Considering the EoM of the parallel mechanism in (12), the interaction forces/torques can be included as,

$$\boldsymbol{f}_a = \mathbf{J}_r^{+T}\left(\boldsymbol{\tau}_{in}+\boldsymbol{\tau}_{patient}\right), \tag{15}$$

where $\boldsymbol{\tau}_{patient}$ is the vector of torques applied by the user to the footplate and $\boldsymbol{\tau}_{in}$ is the vector of torques due to inertia and gravitational effects of the mechanism. Further to this, when the patient needs to perform active exercises, it is necessary to simulate a certain dynamics, via imposing certain inertia, stiffness and damping parameters. Therefore, the torques felt by the patient will be equal to those obtained from the simulation of a mass-spring-damper system as,

$$\boldsymbol{\tau}_{patient} = \boldsymbol{\tau}_{virtual}\,.$$

Hence, the expression in (15) becomes,

$$\boldsymbol{f}_a = \mathbf{J}_r^{+T}(\boldsymbol{\tau}_{in} + \boldsymbol{\tau}_{virtual}), \tag{16}$$

where $\boldsymbol{\tau}_{virtual}$ is the vector of torques necessary to simulate a certain dynamics (see Section V).

IV. Control for Rehabilitation Exercises

The rehabilitation protocol for ankle injuries can be seen in Table I [22]. To permit the effective execution of these regimes the control architecture of the device employs a different control scheme appropriate to the necessities of a particular exercise.

TABLE I
Control Algorithms for Rehabilitation Exercises

Class of exercise	Exercise mode (patient)		Control Algorithms
ROM (Range of Motion)	Passive		Position Control
	Active		Assistive Control
Strength training	Active	Isometric	Position Control
		Isotonic	Admittance Control
Proprioceptive training	Active		Hybrid Control

In the early stage of the therapy, the patient can hardly move his/her foot, therefore a passive exercise which would delicately move the patient's foot is needed.

Such task can be accomplished by a position control scheme which can drive the injured foot/ankle along a certain trajectory at moderate speed. Trajectory parameters, such as wave type, speed, amplitudes and number of repetitions can be set by the physiotherapist. In order to allow the patient to fully regain his/her ROM and to evaluate the patient's progress of the first stage of the rehabilitation, active exercises can also be executed by an assistive control scheme based on admittance techniques. Suppose the patient is capable of providing moderate torque levels to initiate the motion however, he cannot provide enough torque to complete the exercise trajectory. In this case, the application of the patient torque to the footplate can be monitored by the installed FT sensor, therefore providing information to the assistive controller about the patient indentation motion. The assistive control (see Section IV.*C*) supplies the additional torque effort required in order to assist the patient to complete the motion.

The position control algorithm is also used for isometric strengthening exercises. In this case the ankle rehabilitation robot is controlled to maintain a fixed position while the patient tries to apply a certain level of torque to the footplate. The applied torque is measured by the FT sensor and the muscle activation is monitored through the measurement of EMG signals. Strength training includes also isotonic exercises, as in Table I. For this kind of regime, an admittance controller is implemented in order to provide a certain resistance to the patient's motion.

In the last stage of the rehabilitation process, the patient has to undergo proprioceptive training. Balance exercises are typical for this kind of training and in such a case, the patient has to stand on top of the robot and try to keep the balance, as if he/she was using a wobble board. Since the dynamic behavior, position and velocity, can be controlled, more sophisticated exercises can be performed with this system, than those allowed by traditional tools (foam rollers, wobble boards, etc.). Hybrid control (combination of position and force control) can be used to design this type of exercises.

The work presented in this paper focuses on the first two steps of the rehabilitation protocol while proprioceptive training will be treated elsewhere.

A. Patient-passive Exercises

As mentioned above, when the patient is passive the robot is controlled to follow a reference trajectory imposed by the therapist or to hold a certain position. In order to obtain high position tracking accuracy, a computed-torque controller is implemented. The block diagram of the proposed controller is shown in Fig. 4. The EoM introduced in (12) are used to compute the actuation forces required by the parallel mechanism to follow a certain trajectory. An additional torque term $\boldsymbol{\tau}_s$ is added in a feed-forward manner to compensate for the elasticity of the actuator cable transmission system (see actuator model Fig. 3). Hence, the expression of the DC motor torque is

$$\boldsymbol{\tau}_{DC} = \frac{r_p}{\rho}\left[\,\mathbf{J}_r^{+T}\left(\mathbf{M}\left(\ddot{\boldsymbol{q}}_{in_r} + k_P\boldsymbol{e} + k_D\dot{\boldsymbol{e}} + k_I\int \boldsymbol{e}\right)\right.\right. \\ \left.\left. +\mathbf{C}\dot{\boldsymbol{q}}_{in} + \mathbf{N}\right)\right] + \boldsymbol{\tau}_s. \tag{17}$$

From (17) it can be seen that the EoM is used in the control loop to linearize the system and the PID controller is used to compensate for modeling errors and its contribution is added to the reference acceleration. This control scheme allows high position tracking accuracy, if the dynamic model of the robot is well known.

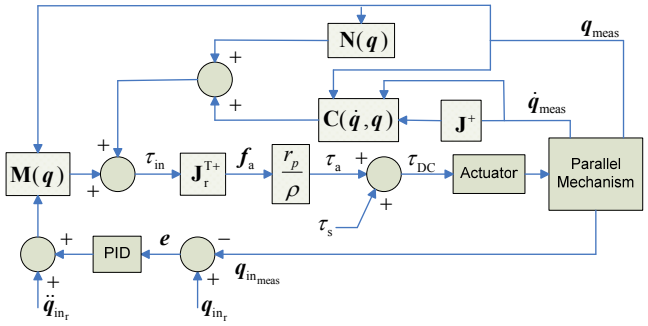

Figure 4. Computed torque control.

B. Patient-Active Exercises: Strengthening

When considering strengthening exercise, two different situations need to be distinguished. As mentioned above, isometric exercises require a fixed position, therefore a computed-torque control algorithm as the one used for patient-passive exercises, can be implemented.

Otherwise, to perform isotonic exercise or other types of resistive training, an admittance control is chosen. As in (16), a certain dynamic behavior of the rehabilitation device can be simulated in relation to the patient-robot interaction.

By measuring the interaction torque applied by the user to the footplate, it is possible to compute the reference position required to simulate certain mass, stiffness and damping parameters. Hence, the reference position $\boldsymbol{q}_{\mathrm{in_r}}$ in Fig. 4 is obtained with an admittance filter as,

$$\boldsymbol{q}_{\mathrm{in_r}} = \frac{\boldsymbol{\tau}_{\mathrm{patient}}}{(ms^2+bs+k)} \ . \tag{18}$$

where m, b and k are the desired mass, damping and spring parameters.

Using the control scheme in Fig. 4, the dynamics expressed by the denominator of (18) can be simulated, since all the other dynamic components are compensated by the computed-torque control.

C. Patient-Active Exercises: Assistance

Assistive control is required in the early stage of rehabilitation when the patient cannot complete the movement alone and needs to reacquire his/her range of motion. If patient's muscles are weak because injured or have not been used due to impairment for a while, assistive ROM training will help them to regain strength. Assistance can be provided with the robot, by measuring patient's effort in terms of either applied torque or muscle activation (via EMG signals) and consequently, providing motion along the direction in which the person is trying to move.

To achieve this, the robot is controlled in position, using the control scheme in Fig. 4. The measured interaction force/torque is integrated over time and used to update the robot reference position, in terms of equilibrium point of a spring damper system, as in Fig. 5.

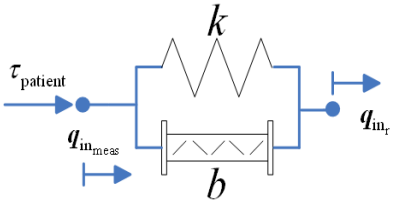

Figure 5. Assistive control model.

In particular the reference position is obtained from,

$$\boldsymbol{q}_{\mathrm{in_r}} = \frac{\boldsymbol{\tau}_{\mathrm{patient}}}{(bs+k)} + \boldsymbol{q}_{\mathrm{as}} \ , \tag{19}$$

with

$$\boldsymbol{q}_{\mathrm{as},k} = \boldsymbol{q}_{\mathrm{as},k-1} + \int_0^t k_{\mathrm{a}} \boldsymbol{\tau}_{\mathrm{patient}} \, \mathrm{d}t \tag{20}$$

where $\boldsymbol{q}_{\mathrm{as}}$ is the assistive component of the position reference and k_{a} is a weight constant that determines the level of assistance. The greater the value of k_{a}, the higher the assistance provided. The torque is measured with the 6-axis FT sensor and the EMG signals are collected to evaluate the patient's effort.

V. Experimental Results

A. Torque-Sensing based Compliant Control

Using the control scheme in Fig. 4 and the expression in (18) a set of experiments was performed in order to evaluate the ability of the system to simulate certain stiffness and damping levels.

The parameters of the simulated compliance filters are given in Table II. Note that, the mass m has been set to zero

TABLE II
COMPLIANCE CONTROL PARAMETERS

Parameter	Stiffness Experiment	Damping Experiment
Mass, m [kg]	0	0
Damping, b [Nm·s·rad^{-1}]	1	0
Stiffness, k [Nm·rad^{-1}]	10, 30, 60, 100	2, 5, 10, 20

TABLE III
COMPLIANCE CONTROL RESULTS - STIFFNESS

Desired Stiffness [Nm·rad^{-1}]	Measured Stiffness [Nm·rad^{-1}]	Error %
10	10.08	0.8
30	29.7	1
60	59.12	1.47
100	94.6	5.4

TABLE IV
COMPLIANCE CONTROL RESULTS - DAMPING

Desired Damping [Nm·s·rad^{-1}]	Measured Damping [Nm·s·rad^{-1}]	Error %
2	1.95	2.5
5	4.99	0.2
10	9.98	0.2
20	20.72	3.6

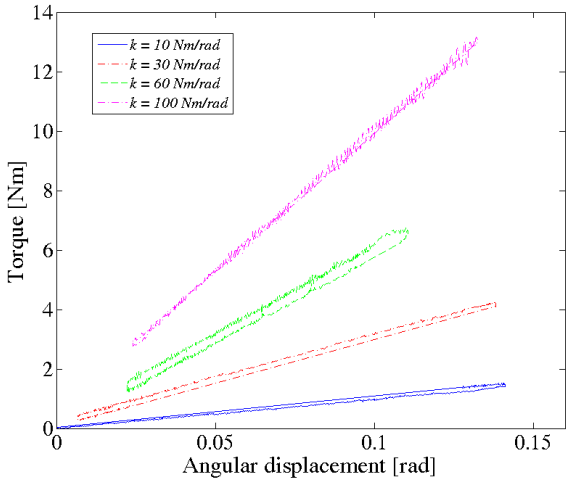

Figure 6. Simulation of stiffness.

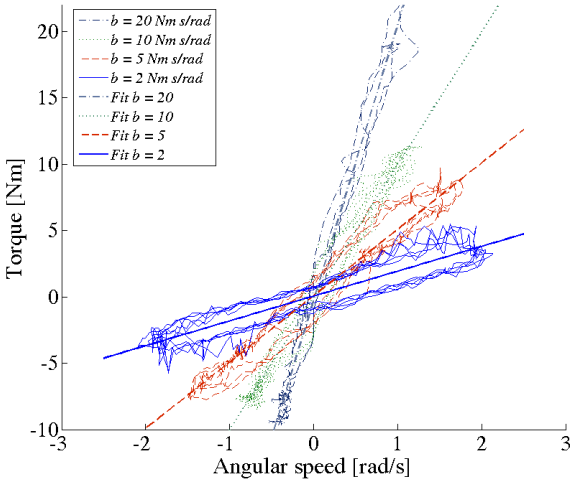

Figure 7. Simulation of damping.

and, in the case of *pure* stiffness simulation, a small damping was necessary to guaranty system stability. The experiments have been performed with low speeds (when simulating *pure* stiffness).

The results are shown in Fig. 6 and 7 and reported in Tables III and IV. The graphs report the measured torque applied by the user to the footplate versus the platform position and velocity computed through the forward kinematics from the measured limb lengths. It is possible to see that the stiffness perceived by the user, Fig. 6 and Table III, is close to the reference stiffness value. Table III reports the slopes of the curves shown in the graph.

Looking at the last column of Table III is evident that the robot performance decreases with the increase of desired stiffness. However, there is no evidence in the literature suggesting that higher accuracies than those achieved are required for rehabilitation exercises, therefore an error of 5.4% as in the last case is acceptable.

Figure 7 shows the results for the simulation of damping. The noise that can be observed in the curves is due to the numerical derivation of the angular position. It can be seen in Table IV that the efficacy of the robot in simulating damping is high for all the reference damping values.

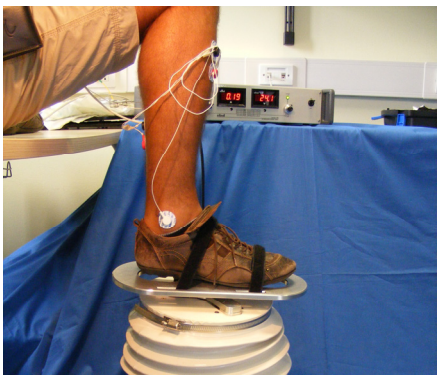

Figure 8. Subject's leg with two pairs of electrodes for EMG signals collection

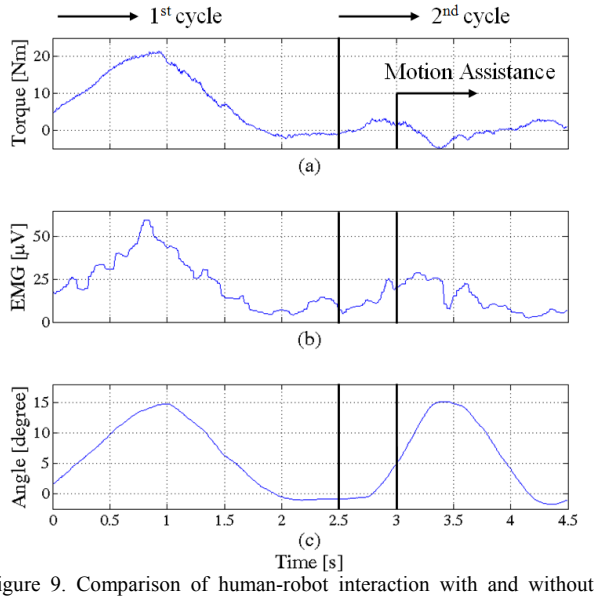

Figure 9. Comparison of human-robot interaction with and without assistive control.

B. *Torque-Sensing based Assistive Control*

The next experiment was conducted in order to evaluate the proposed assistive control algorithm. A young male subject was asked to perform the experiment. The subject right foot was constrained to the footplate and two pairs of electrodes were applied to his leg to measure the muscle activity during motion, see Fig. 8.

The trial consisted in extending and contracting the foot to reach 15 degrees of maximum extension and return back to the start position, twice. During the first extension/flexion cycle the subject experienced a counteracting torque due to the compliance parameters been set to k = 80Nm·rad^{-1} and b = 8Nm·s·rad^{-1}. In the second cycle the assistive control component described in (19, 20) was introduced. The results of this experiment can be seen in Fig. 9.

Figure 9(a) reports the human-robot interaction torque, while Fig. 9(b) and (c) the EMG signal and the angular displacement of the foot/platform, respectively.

It is possible to notice that, during the first cycle the subject has to provide a certain effort in terms of muscle activity, Fig. 9(b), and this is reflected by the amount of interaction torque, Fig. 9(a).

Differently, in the second cycle the subject had to provide a definitely smaller muscle effort to begin the motion. Consequently, the assistive control becomes active and starts pushing the subject's foot in the direction he previously started the movement. This can be also observed from the interaction torque relative to the second cycle, since it initially increases and subsequently decreases, becoming negative. The negative value of interaction torque proves the *pushing* effect of the assistive control.

VI. Discussion and Conclusions

The experimental results effectively demonstrated the good performance of the ankle rehabilitation system and its control scheme. Such rehabilitative device can have a great impact in improving diagnosis and physiotherapy outcomes in ankle rehabilitation.

The control algorithms presented in this study will serve as framework for the design and development of patient-oriented rehabilitation exercises. Future work will look at the development of rehabilitation exercises in collaboration with a team of clinicians and the integration of a virtual environment to stimulate the patient during training.

In conclusion, this paper presented the design of control algorithms for a high performance parallel robot used for robot-aided ankle exercises. The rehabilitation protocol has been considered as the basis for the design of control strategies. Both patient-passive and active exercise types have been addressed using position and admittance control strategies. Further, the EMG signals have been introduced in the control system with the purpose of monitoring the patient's effort and evaluating the effectiveness of the proposed assistive control. The experimental results of stiffness/damping simulation and assisted motion proved the high performance of the rehabilitation device and showed the great potential of such a robot in improving the result of physiotherapy.

References

[1] H.I. Krebs, N. Hogan, M.L. Aisen, and B.T. Volpe, "Robot-aided neurorehabilitation," IEEE Transactions on Rehabilitation Engineering, vol.6, no.1, pp.75-87, Mar 1998.

[2] B.T. Volpe, H.I. Krebs and N. Hogan, "Is robot-aided sensorimotor training in stroke rehabilitation a realistic option?", Current Opinion in Neurology, Vol. 14, No. 6, pp 745-752, December 2001.

[3] P.S. Lum, C.G. Burgar, P.C. Shor, M. Majmundar, M. Van der Loos, "Robot-Assisted Movement Training Compared With Conventional Therapy Techniques for the Rehabilitation of Upper-Limb Motor Function After Stroke," Archives of Physical Medicine and Rehabilitation, Vol. 83, No. 7, pp. 952-959, July 2002.

[4] J. Hidler, D. Nichols, M. Pelliccio and K. Brady, "Advances in the Understanding and Treatment of Stroke Impairment Using Robotic Devices," Topics in Stroke Rehabilitation, Vol. 12, No. 2, pp. 22–35, Spring 2005.

[5] H.I. Krebs, B.T. Volpe, M.L. Aisen and N. Hogan, "Increasing productivity and quality of care: Robot-aided neuro-rehabilitation," Journal of Rehabilitation Research and Development, Vol. 37, No. 6, pp. 639-652, November/December 2000.

[6] S.E. Fasoli, H.I. Krebs, J. Stein, W.R. Frontera, R. Hughes and N. Hogan, "Robotic Therapy for Chronic Motor Impairments After Stroke: Follow-Up Results," Archives of physical medicine and rehabilitation, Vol. 85, No. 7, pp. 1106-11, July 2004.

[7] M. Hillman, "Rehabilitation Robotics from Past to Present – A Historical Perspective," Proceedings of the ICORR 2003 (The Eighth International Conference on Rehabilitation Robotics), 23-25 April 2003.

[8] M.-S. Ju, C.-C. K. Lin, D.-H. Lin, I.-S. Hwang, and S.-M. Chen, "A Rehabilitation Robot with Force-Position Hybrid Fuzzy Controller: Hybrid Fuzzy Control of Rehabilitation Robot," IEEE Transactions on Neural Systems and Rehabilitation Engineering, Vol.13, No.3, pp. 349-358, September 2005.

[9] D. Formica, L. Zollo and E. Guglielmelli, "Torque-dependent Compliance Control in the Joint Space of an Operational Robotic Machine for Motor Therapy," 9th International Conference on Rehabilitation Robotics, pp. 341-344, 28 June-1 July 2005.

[10] D.P. Ferris, K.E. Gordon, G. S. Sawicki and A. Peethambaran, "An improved powered ankle–foot orthosis using proportional myoelectric control," Gait & posture, Vol. 23, No. 4, pp. 425-428, June 2006.

[11] R. Song, K.-y. Tong, X. Hu and L. Li, "Assistive Control System Using Continuous Myoelectric Signal in Robot-Aided Arm Training for Patients After Stroke," IEEE Transactions on Neural Systems and Rehabilitation Engineering, Vol.16, No.4, pp. 371-379, August 2008.

[12] M. DiCicco, L. Lucas and Y. Matsuoka, "Comparison of control strategies for an EMG controlled orthotic exoskeleton for the hand," Proceedings of IEEE ICRA, pp. 1622-1627, April 26-May 1, 2004.

[13] N. Hogan, "Impedance control - An approach to manipulation. I - Theory. II - Implementation. III - Applications," ASME, Transactions, Journal of Dynamic Systems, Measurement, and Control, Vol. 107, March 1985, pp. 1-24.

[14] M. J. Girone, G. C. Burdea and M. Bouzit, "The Rutgers Ankle Orthopedic Rehabilitation Interface," ASME Int. Mechanical Engineering Congress and on Dynamic Systems and Control Division, Nashville TN, November 1999, Vol. 67, pp. 305-312.

[15] M. Girone, G. Burdea, M. Bouzit, and J. Deutsch, "Orthopedic rehabilitation using the 'Rutgers Ankle' interface," Proceedings of Medicine Meets Virtual Reality, IOS Press, pp. 89–95, January 2000.

[16] M. Girone, G. Burdea, M. Bouzit, V. Popescu and J. Deutsch, "A Stewart platform-based system for ankle telerehabilitation," Autonomous Robots, Vol. 10, pp. 203–212, 2001.

[17] J. Deutsch, J. Latonio, G. Burdea and R. Boian, "Rehabilitation of musculoskeletal injuries using the Rutgers ankle haptic interface: three case reports," Eurohaptics Conference, Birmingham, UK, July 2001.

[18] J. Yoon, J. Ryu, "A Novel Reconfigurable Ankle/Foot Rehabilitation Robot," Proc. of IEEE ICRA, pp. 2290-2295, April 18-22, 2005.

[19] C.-C. K. Lin, M.-S. Ju, S.-M. Chen and B.-W. Pan, "A Specialized Robot for Ankle Rehabilitation and Evaluation," Journal of Medical and Biological Engineering, Vol. 28, No.2, pp. 79-86, 2008.

[20] G. Liu, J. Gao, H. Yue, X. Zhang and G. Lu, "Design and Kinematics Analysis of Parallel Robots for Ankle Rehabilitation," Proceedings of the IEEE/RSJ IROS , Beijing, pp. 253-258, October 9 – 15, 2006.

[21] J.A. Saglia, N.G. Tsagarakis, J.S. Dai and D.G. Caldwell, "A High Performance 2-dof Over-Actuated Parallel Mechanism for Ankle Rehabilitation", Proceedings of IEEE ICRA, Kobe, Japan, May 2009.

[22] J.A. Saglia, N.G. Tsagarakis, J.S. Dai and D.G. Caldwell, "A High Performance Redundantly Actuated Parallel Mechanism for Ankle Rehabilitation," The International Journal of Robotics Research, SI on Medical Robotics, Vol. 28, No. 9, September 2009, pp. 1216–1227.

[23] J. Saglia, J.S. Dai and D.G. Caldwell, "Geometry and Kinematic Analysis of a Redundantly Actuated Parallel Mechanism that Eliminates Singularity and Improves Dexterity," Transactions of the ASME: Journal of Mechanical Design, vol. 130, no. 12, page 124501_1-5, 2008.

[24] H. Cheng, G.F. Liu, Y.K. Yiu, Z.H. Xiong, Z.X. Li, "Advantages and dynamics of parallel manipulators with redundant actuation," Proc. of the IEEE/RSJ IROS, Maui, Hawaii, USA, pp.171-176, 2001.

[25] H. Cheng, Y.-K. Yiu, Z. Li, "Dynamics and control of redundantly actuated parallel manipulators," IEEE/ASME Transactions on Mechatronics, Vol.8, No. 4, pp.483-491, December 2003.

[26] M. ValÁšek, V. Bauma, Z. šika, K. Belda and P. PÍša, "Design-by-Optimization and Control of Redundantly Actuated Parallel Kinematics Sliding Star," Multibody System Dynamics, Vol. 14, No. 3-4, November 2005 , pp. 251-267.

[27] J.A. Saglia, N.G. Tsagarakis, J.S. Dai and D.G. Caldwell, "Inverse-Kinematics-Based Control of a Redundantly Actuated Platform for Rehabilitation," Journal of Systems and Control Engineering, IMechE Proceedings, Part I, vol. 223, no.1, page 53-70, 2009.